Transport and Communications Science Journal, Vol. 75, Issue 07 (09/2024), 2015-2029

Transport and Communications Science Journal

BENDING AND BUCKLING RESPONSES OF ORGANIC NANOPLATES CONSIDERING THE SIZE EFFECT

Dao Minh Tien[1,2], Do Van Thom[3*], Phung Van Minh[3], Pham Huy Hieu[2]

[1]Graduate University of Science and Technology, Vietnam Academy of Science and Technology, No. 18 Hoang Quoc Viet Street, Cau Giay, Hanoi, Vietnam

[2]Air Force-Air Defence Technical Institute, Hanoi, Vietnam

[3]Faculty of Mechanical Engineering, Le Quy Don Technical University, No. 236 Hoang Quoc Viet Street, Hanoi, Vietnam.

ARTICLE INFO

TYPE: Research Article
Received: 28/05/2024
Revised: 25/06/2024
Accepted: 10/09/2024
Published online: 15/09/2024
https://doi.org/10.47869/tcsj.75.7.1

[*] *Corresponding author*
Email: thom.dovan.mta@gmail.com

Abstract. As humanity progresses, fossil fuel reserves are being increasingly exhausted, leading to increased focus on sustainable energy alternatives. Scientists are now researching solar panels that can efficiently convert solar energy into electricity for human use. This research employs a novel third-order shear deformation theory to investigate the static buckling and static bending behaviors of organic nanoplates, marking the first instance of such an approach being used. The formulas are computed using strain gradient theory to consider the impact of the size effect, where this size effect parameter is considered in both positive and negative cases. The plate's balancing equation is derived using the notion of virtual displacement, and the analytical solution is obtained using Navier's solution. The mathematical expression for deflection and critical buckling load in this study has been validated by comparing it with previously published analytical findings. This study also includes a set of numerical calculations to demonstrate the impact of certain geometric factors and the size effect on the static bending response and static buckling of organic plates. This study aims to assist designers in developing organic plate products that demonstrate optimal functionality in real-world applications.

Keywords: bending; buckling; nanoplates; Navier solution; nonlocal theory; Organic solar cells.

1. INTRODUCTION

With the expansion of modern society, environmental pollution has emerged as a global concern, leading to substantial alterations in people's lifestyles. In order to reduce environmental pollution, individuals have been actively seeking and using novel materials and clean, renewable energy sources. Solar energy is a prominent kind of energy that is garnering considerable attention. Solar energy is a feasible choice due to its non-polluting nature and its ability to be promptly gathered and used. Furthermore, it does not release any potentially hazardous byproducts. Organic solar cells (OSCs) have become more popular owing to their many favorable features [1]. The qualities include their affordable cost, straightforward production process, nanoscale dimensions, and compact form. Consequently, organic solar cells (OSCs) have been extensively used in many industries such as aerospace, automotive sector for new energy, and building-integrated photovoltaics (BIPV) [2]. Conversely, the OSCs must operate in conditions characterized by varying levels of natural light, moisture, and temperature fluctuations. It is essential for all OSC devices to possess sufficient compression resistance; otherwise, they will succumb to buckling and malfunction before to their designated service life [3].

To enhance the efficacy of using OSCs, it is essential to possess comprehensive knowledge in several domains, such as picking the material, size choosing, mechanical response, and others. Therefore, scientific society has shown enthusiasm for the examination of OSC as a result of this. These attempts include optimizing the electrode substance [4], enhancing the internal structure [5], and choosing suitable production materials [6]. The majority of these investigations focused on the efficacy of various materials. Additionally, the devices are fabricated from OSC often suffer from physical harm when used in real-world scenarios. As power equipment worn on the skin, they must possess the ability to withstand substantial bending and compression [6]. When dealing with structures like OSC, which have small dimensions in the micron and nanometer spectrum, it is important to note that both the properties of the material and the mechanical behavior of the devices will experience significant changes. These updates will happen simultaneously. Research in the past few years has seen significant growth in both study and practical application, aiming to enhance the precision of predictions about the mechanical properties of microstructures. This is the premise to create products with high practical applications and this product has the best usage efficiency. When calculating small-sized structures, one can use many non-classical continuum theories, including the nonlocal elasticity hypothesis, the revised couple stress concept, and the modified strain gradient hypothesis [7-10]. Qingya and colleagues [11] used an enhanced version of the plate theory and an updated strain gradient model to explore the influence of size effect on free vibration and static bending. In this study, Qingya et al. [12] use the revised strain gradient theory and the revised shear deformation plate theory to examine the buckling characteristics of simply supported and clamped OSC structures. The objective of this experiment was to investigate the causes and mechanisms behind the failure of the OSC. Duc et al. [13] provide the first analytical approach for investigating the nonlinear dynamic behavior and vibration of imperfect nanocomposite multilayer solar cells subjected to mechanical pressures, using the traditional plate theory. The theory's errors arise from its initial development using defective rectangular nanocomposite multilayer organic solar cells and its inability to consider the influence of size factors on the plate's behavior. Liu and colleagues [14] used an efficient isogeometric technique and a couple stress theory to examine the influence of size on the thermomechanical operation of organic solar cells.

Furthermore, results of mechanical studies are consistently generating a diverse array of theories and instruments to research the mechanical properties of structures at the nano and micro levels. This establishes a crucial foundation for the advancement of solar thermal cell development. The following works serve as sample instances of recently published publications. Hamed and Masoud [15] used first-order shear strain theory and analytical methodologies to examine the buckling of nanoplates. They ensured to examine the influence of both the size effect and the flexomagnetic effect. Furthermore, Naderi [16] employs the Navier product solution to address the buckling problem of nano-sized plates, using the three-dimensional elastic theory. Esen and Ozmen [17] used Navier's solution in combination with first-order shear strain theory to analyze the vibration and buckling of nanoplates. Jin and Ren [18] investigated the issue of forced vibration caused by bending in nanoplates using Zhang-Fu's theory. This theory included both the influence of surface energy and the impact of size. In their work, Hai et al. [19] used an enhanced strain theory and analytical techniques to examine how the size effect impacts the compelled oscillation of composite nanoplates that are supported by viscoelastic substrates. The external force applied to the plate in this scenario is a moving load. Tuyen [20] utilizes the vibration of the nano-plate on the viscoelastic foundation to present a solution for the nanoplate. This solution takes into account the effects of temperature and flexoelectricity. The balanced equation is established using classical theory and it was solved by exact approach. In their study, Wan et al. [21] examined the buckling, free vibrations, and forced vibrations of nano-sized composite plates. These plates were supported by viscoelastic substrates and analyzed using the Halpin-Tsai theory. Luat and colleagues [22] analyzed the vibration, buckling and bending behavior of a composite nanobeam using a new shear deformation concept. The sandwich beam, including a ceramic core and two face sheets with functional grading, has considerable potential for many applications in engineering and industry. Duc et al. [23] used finite element modeling (FEM) together with a unique shear deformation theory based on a hyperbolic sine function to investigate the vibration response and static buckling of variable flexoelectric nanoplates. Both linear and nonlinear methodologies were used to modify the thickness of the nanoplates. Doan and colleagues [24] successfully investigated the vibration behavior of nano-plates by combining the concept of a high-order plate theory with the phase-field approach. By considering the flexoelectric effect, he successfully included the interdependent connection between charge polarization and strain. Shear connections were required for the sliding movement between the layers, and Thai et al. [25] conducted a static bending study of symmetric three-layer functionally graded sandwich beams. The beam equilibrium equation was developed using a combination of the finite element approach and the first-order beam theory (FSDT) and, resulting in finite element formulations. Thom and his colleagues [26], [27] subsequently provided new numerical findings about the vibration response of a fragmented FGM plate. The research used the finite element approach and phase-field theory.

From the above information, it is evident that there has been no study conducted on assessing the mechanical response of organic plate frameworks employing strain gradient concept to consider the small-size impact. Hence, this study addresses this issue by using analytical techniques. The precise resolution to the problem of static bending and static buckling of biological plates is achieved by employing the concept of the enhanced third-order shear deformation theory.

2. CALCULATION MODEL, METHOD AND SOLUTION

Fig. 1 displays the organic nanoplate model, situated inside the Cartesian *XYZ* coordinate system. The variables *a* and *b* represent the dimensions of the model, namely its length and breadth, respectively. The nanoplate has five layers, with each layer having a distinct thickness denoted by the notation h_i.

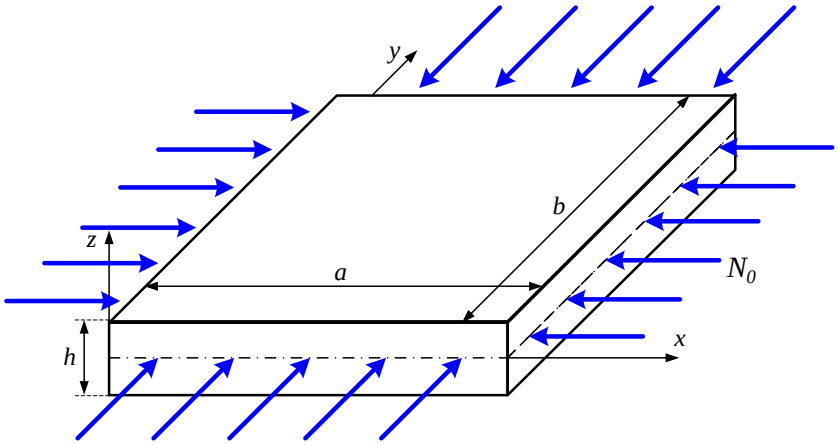

a) General model

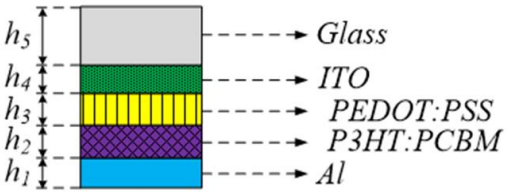

b) zy cross-section

Figure 1. An organic nanoplate model [28].

When calculating plate and shell structures, it is common practice to express the displacement components along the three Cartesian coordinate axes using different functional forms. Every kind of function has certain advantages and disadvantages. Although challenging to compute, functional forms accurately depict the mechanical response of structures, especially as their intricacy grows. Furthermore, this research employs three separate types of functions to compute the displacement components along the Ox and Oy coordinate axes. Moreover, this work utilizes a functional form to calculate the displacement component along the Oz coordinate axis. The form of the displacement field along the three Cartesian coordinate axes may be represented as follows:

$$\begin{Bmatrix} u_x \\ v_y \\ w_z \end{Bmatrix} = \begin{Bmatrix} 0 \\ 0 \\ w_{zb} + w_{zs} \end{Bmatrix} - z\left\{\frac{\partial w_{zb}}{\partial x}, \frac{\partial w_{zb}}{\partial y}, 0\right\}^T - g_z\left\{\frac{\partial w_{zs}}{\partial x}, \frac{\partial w_{zs}}{\partial y}, 0\right\}^T \quad (1)$$

The variables u_x, v_y, and w_z indicate the displacement components along the *x*- , *y*- and *z*-coordinate axes. The variable w_{zb} and w_{zs} represent the bending and shear components. The g_z function is [29]:

$$g_z = -z/4 + 5z^3/3h^2 \tag{2}$$

From the expression of displacement field as (2), the components of strain are:

$$\begin{aligned} &\varepsilon_{zx} = -\frac{\partial^2 w_{zb}}{\partial x^2};\ \varepsilon_{zy} = -\frac{\partial^2 w_{zb}}{\partial y^2};\ \gamma_{zxy} = -2\frac{\partial^2 w_{zb}}{\partial x \partial y};\ \varepsilon_{gx} = -\frac{\partial^2 w_{zs}}{\partial x^2};\ \varepsilon_{gy} = -\frac{\partial^2 w_{zs}}{\partial y^2}; \\ &\gamma_{gxy} = -2\frac{\partial^2 w_{zs}}{\partial x \partial y};\gamma_{sxz} = \frac{\partial w_{zs}}{\partial x};\ \gamma_{syz} = \frac{\partial w_{zs}}{\partial y} \end{aligned} \tag{3}$$

Equation (3) is written in reduced form as:

$$\boldsymbol{\varepsilon} = z\boldsymbol{\varepsilon}_z + g_z\boldsymbol{\varepsilon}_e;\ \boldsymbol{\gamma}_s = k_z\boldsymbol{\gamma}_{s0} \tag{4}$$

in which $k_z = 1 - dg_z/dz$ and

$$\boldsymbol{\varepsilon}_z = \left\{\varepsilon_{zx}, \varepsilon_{zy}, \varepsilon_{zxy}\right\}^T;\ \boldsymbol{\varepsilon}_e = \left\{\varepsilon_{gx}, \varepsilon_{gy}, \varepsilon_{gxy}\right\}^T;\ \boldsymbol{\gamma}_{s0} = \left\{\gamma_{sxz}, \gamma_{syz}\right\}^T \tag{5}$$

Typically, the earlier studies do not include the structural resistance of the structure. This results in a divergence between the theoretical calculation and the experience. The stress components in the *i*-th layer, which are calculated using nonlocal theory, may be expressed as follows [30-31]:

$$\sigma_{mn}^i = \beta_{mnkq}^i\left(1 \pm l^2\nabla^2\right)\varepsilon_{kq}^i;\quad \tau_{rj}^i = \beta_{rj}^i\left(1 \pm l^2\nabla^2\right)\gamma_{rj}^i \tag{6}$$

In this context, l denotes the nonlocal parameter; "+" and "-" indicate positive and negative nonlocal parameters, respectively; ∇^2 represents the Laplace operator; σ_{mn}^i represents the stress tensor; and β_{mnkq}^i represents the elastic tensor, which comprises the material parameters.

Equation (6) is expanded in the following manner:

$$\boldsymbol{\sigma}^i = \begin{Bmatrix}\sigma_x \\ \sigma_y \\ \sigma_{xy}\end{Bmatrix}^i = \begin{bmatrix}\beta_{11}^i & \beta_{12}^i & 0 \\ \beta_{12}^i & \beta_{11}^i & 0 \\ 0 & 0 & \beta_{33}^i\end{bmatrix}\begin{Bmatrix}\varepsilon_x \\ \varepsilon_y \\ \gamma_{xy}\end{Bmatrix}^i = \boldsymbol{\beta}_b^i\left(1 - l^2\nabla^2\right)\boldsymbol{\varepsilon}^i \tag{7a}$$

$$\boldsymbol{\tau}^i = \begin{Bmatrix}\tau_{xz} \\ \tau_{yz}\end{Bmatrix}^i = \begin{bmatrix}\beta_{33}^i & 0 \\ 0 & \beta_{33}^i\end{bmatrix}\begin{Bmatrix}\gamma_{xz} \\ \gamma_{yz}\end{Bmatrix}^i = \boldsymbol{\beta}_s^i\left(1 - l^2\nabla^2\right)\boldsymbol{\gamma}_s^i \tag{7b}$$

utilizing the following material properties for the *i*-th layer:

$$\beta_{11}^i = \frac{E_i}{1-\nu_i^2};\ \beta_{12}^i = \nu_i\beta_{11}^i;\ \beta_{33}^i = \frac{E_i}{2\left(1+\nu_i\right)};\ \boldsymbol{\beta}_b^i = \begin{bmatrix}\beta_{11}^i & \beta_{12}^i & 0 \\ \beta_{12}^i & \beta_{11}^i & 0 \\ 0 & 0 & \beta_{33}^i\end{bmatrix};\ \boldsymbol{\beta}_s^i = \begin{bmatrix}\beta_{33}^i & 0 \\ 0 & \beta_{33}^i\end{bmatrix} \tag{8}$$

The following are the internal forces of the plate as determined by Equation (7):

$$\begin{Bmatrix} M_x \\ M_y \\ M_{xy} \end{Bmatrix} = \sum_i \int_{h_i}^{h_{i+1}} \begin{bmatrix} \beta_{11}^i & \beta_{12}^i & 0 \\ \beta_{12}^i & \beta_{11}^i & 0 \\ 0 & 0 & \beta_{33}^i \end{bmatrix} \begin{Bmatrix} \varepsilon_x \\ \varepsilon_y \\ \gamma_{xy} \end{Bmatrix}^i z dz - l^2\nabla^2 \sum_i \int_{h_i}^{h_{i+1}} \begin{bmatrix} \beta_{11}^i & \beta_{12}^i & 0 \\ \beta_{12}^i & \beta_{11}^i & 0 \\ 0 & 0 & \beta_{33}^i \end{bmatrix} \begin{Bmatrix} \varepsilon_x \\ \varepsilon_y \\ \gamma_{xy} \end{Bmatrix}^i z dz \tag{9a}$$

$$= \boldsymbol{A}\boldsymbol{\varepsilon}_z + \boldsymbol{B}\boldsymbol{\varepsilon}_g - l^2\nabla^2 \boldsymbol{A}\boldsymbol{\varepsilon}_z - l^2\nabla^2 \boldsymbol{B}\boldsymbol{\varepsilon}_g$$

$$\begin{Bmatrix} T \\ T_y \\ T_{xy} \end{Bmatrix} = \sum_i \int_{h_i}^{h_{i+1}} \begin{bmatrix} \beta_{11}^i & \beta_{12}^i & 0 \\ \beta_{12}^i & \beta_{11}^i & 0 \\ 0 & 0 & \beta_{33}^i \end{bmatrix} \begin{Bmatrix} \varepsilon_x \\ \varepsilon_y \\ \gamma_{xy} \end{Bmatrix}^i g_z dz - l^2\nabla^2 \sum_i \int_{h_i}^{h_{i+1}} \begin{bmatrix} \beta_{11}^i & \beta_{12}^i & 0 \\ \beta_{12}^i & \beta_{11}^i & 0 \\ 0 & 0 & \beta_{33}^i \end{bmatrix} \begin{Bmatrix} \varepsilon_x \\ \varepsilon_y \\ \gamma_{xy} \end{Bmatrix}^i g_z dz \tag{9b}$$

$$= \boldsymbol{B}\boldsymbol{\varepsilon}_z + \boldsymbol{D}\boldsymbol{\varepsilon}_g - l^2\nabla^2 \boldsymbol{B}\boldsymbol{\varepsilon}_z - l^2\nabla^2 \boldsymbol{D}\boldsymbol{\varepsilon}_g$$

$$\begin{Bmatrix} Q_{xz} \\ Q_{yz} \end{Bmatrix} = \sum_i \int_{h_i}^{h_{i+1}} \begin{bmatrix} \beta_{33}^i & 0 \\ 0 & \beta_{33}^i \end{bmatrix} \begin{Bmatrix} \gamma_{xz} \\ \gamma_{yz} \end{Bmatrix}^i dz - l^2\nabla^2 \sum_i \int_{h_i}^{h_{i+1}} \begin{bmatrix} \beta_{33}^i & 0 \\ 0 & \beta_{33}^i \end{bmatrix} \begin{Bmatrix} \gamma_{xz} \\ \gamma_{yz} \end{Bmatrix}^i dz \tag{9c}$$

$$= \boldsymbol{H}\boldsymbol{\gamma}_{s0} - l^2\nabla^2 \boldsymbol{H}\boldsymbol{\gamma}_{s0}$$

where

$$\{\boldsymbol{A},\boldsymbol{B},\boldsymbol{D}\} = \sum_i \int_{h_i}^{h_{i+1}} \begin{bmatrix} \beta_{11}^i & \beta_{12}^i & 0 \\ \beta_{12}^i & \beta_{11}^i & 0 \\ 0 & 0 & \beta_{33}^i \end{bmatrix}^i \left\{z^2, z g_z, g_z^2\right\} dz \; ; \; \boldsymbol{H} = \sum_i \int_{h_i}^{h_{i+1}} \begin{bmatrix} \beta_{33}^i & 0 \\ 0 & \beta_{33}^i \end{bmatrix} k_z^2 dz \tag{10}$$

By employing the notion of potential motion, the researchers of this investigation obtained the subsequent balanced equation pertaining to organic nanoplates:

$$\delta W_{ngl} - \delta W_{nl} = 0 \tag{11}$$

where δW_{ngl} and δW_{nl} represent the work performed by the external force and internal deformation of the plate, respectively.

The following represents the potential work of an external force acting on the structure:

$$\begin{aligned} \delta W_{ngl} &= \int_{\Omega} p\delta w_z dA - \int_S N_0 \left\{ \left(\frac{\partial w_z}{\partial x}\right)\left(\frac{\partial \delta w_z}{\partial x}\right) + \left(\frac{\partial w_z}{\partial y}\right)\left(\frac{\partial \delta w_z}{\partial y}\right) \right\} dS \\ &= \int_{\Omega} p\delta\left(w_{zb} + w_{zs}\right) d\Omega - \int_S N_0 \left\{ \left(\frac{\partial w_z}{\partial x}\right)\left(\frac{\partial \delta w_z}{\partial x}\right) + \left(\frac{\partial w_z}{\partial y}\right)\left(\frac{\partial \delta w_z}{\partial y}\right) \right\} dS \end{aligned} \tag{12}$$

where p represents the force that acts at a right angle to the plate, whereas N_0 represents the compressive force that acts in the average plane of the plate.

The potential work exerted by the internal force of organic nanoplates may be calculated using the following method:

$$\delta W_{nl} = \int_{\Omega} \sum_{i} \int_{h_i}^{h_{i+1}} \begin{pmatrix} \delta(\varepsilon_x)^i (\sigma_x)^i + \delta(\varepsilon_y)^i (\sigma_y)^i + \delta(\varepsilon_{xy})^i (\sigma_{xy})^i \\ +\delta(\gamma_{xz})^i (\tau_{xz})^i + \delta(\gamma_{yz})^i (\tau_{yz})^i \end{pmatrix} dz d\Omega$$

$$= \int_{\Omega} \sum_{i} \int_{h_i}^{h_{i+1}} \begin{pmatrix} -M_x \frac{\partial^2 \delta w_{zb}}{\partial x^2} - T_x \frac{\partial^2 \delta w_{zs}}{\partial x^2} - M_y \frac{\partial^2 \delta w_{zb}}{\partial y^2} - T_y \frac{\partial^2 \delta w_{zs}}{\partial y^2} \\ -2M_{xy} \frac{\partial^2 \delta w_{zb}}{\partial x \partial y} - 2T_{xy} \frac{\partial^2 \delta w_{zs}}{\partial x \partial y} + Q_{xz} \frac{\partial \delta w_{zs}}{\partial x} + Q_{yz} \frac{\partial \delta w_{zs}}{\partial y} \end{pmatrix} dz d\Omega \quad (13)$$

Through the substitution of equations (12)-(13) into equation (11), the present study derives the subsequent balanced equation describing organic nanoplates:

$$\delta w_{zb} : \frac{\partial^2 M_x}{\partial x^2} + 2\frac{\partial^2 M_{xy}}{\partial x \partial y} + \frac{\partial^2 M_y}{\partial y^2} + p - N_0 \left(\frac{\partial^2 w_z}{\partial x^2} + \frac{\partial^2 w_z}{\partial y^2} \right) = 0 \quad (14)$$

$$\delta w_{zs} : \frac{\partial^2 T_x}{\partial x^2} + 2\frac{\partial^2 T_{xy}}{\partial x \partial y} + \frac{\partial^2 T_y}{\partial y^2} + \frac{\partial Q_{xz}}{\partial x} + \frac{\partial Q_{yz}}{\partial y} + p - N_0 \left(\frac{\partial^2 w_z}{\partial x^2} + \frac{\partial^2 w_z}{\partial y^2} \right) = 0 \quad (15)$$

This study employs a double trigonometric series solution to address the static bending issue of an organic plate, with the exclusion of the compressive force N_0. The answer is presented in the following form:

$$\begin{aligned} w_{zb} &= \sum_{m=1}^{\infty} \sum_{n=1}^{\infty} U_{0b} \sin\left(r\frac{\pi}{a}x \right) \sin\left(g\frac{\pi}{b}y \right) \\ w_{zs} &= \sum_{m=1}^{\infty} \sum_{n=1}^{\infty} U_{0s} \sin\left(r\frac{\pi}{a}x \right) \sin\left(g\frac{\pi}{b}y \right) \\ q &= \sum_{m=1}^{\infty} \sum_{n=1}^{\infty} \frac{16Q_0}{\pi^2 rg} \sin\left(r\frac{\pi}{a}x \right) \sin\left(g\frac{\pi}{b}y \right) \end{aligned} \quad (16)$$

Let r and g be integers. U_{0b} and U_{0s} represent the amplitudes of the displacement components, respectively. By substituting solution (16) into the equations (14)-(15), the resulting expression is obtained:

$$\begin{aligned} &-A_{11}U_{0b}\left(\alpha^4 + \beta^4\right) - 2\left(A_{12} + 2A_{33}\right)U_{0b}\alpha^2\beta^2 \\ &-B_{11}U_{0s}\left(\alpha^4 + \beta^4\right) - 2\left(B_{12} + 2B_{33}\right)U_{0s}\alpha^2\beta^2 \\ &-l^2 \begin{bmatrix} \left(A_{11} + A_{12}\right)U_{0b}\alpha^6 + A_{11}U_{0b}\beta^6 + \left(A_{11} + 2A_{12} + 4A_{33}\right)U_{0b}\alpha^4\beta^2 \\ +\left(A_{11} + A_{12} + 4A_{33}\right)U_{0b}\alpha^2\beta^4 \\ +\left(B_{11} + B_{12}\right)U_{0s}\alpha^6 + B_{11}U_{0s}\beta^6 + \left(B_{11} + B_{12} + 4l^2B_{33}\right)U_{0s}\alpha^2\beta^4 \\ +\left(B_{11} + 2B_{12} + 4l^2B_{33}\right)U_{0s}\alpha^4\beta^2 \end{bmatrix} \\ &+\frac{16Q_0}{\pi^2 rg} + N_0\left(U_{0b} + U_{0s}\right)\left(\alpha^2 + \beta^2\right) = 0 \end{aligned} \quad (17a)$$

$$
\begin{aligned}
&-B_{11}U_{0b}\left(\alpha^4+\beta^4\right)-2\left(B_{12}+2B_{33}\right)U_{0b}\alpha^2\beta^2\\
&-\left(D_{11}+H_{33}l^2\right)U_{0s}\left(\alpha^4+\beta^4\right)-2\left(D_{12}+2D_{33}+H_{33}l^2\right)U_{0s}\alpha^2\beta^2\\
&-l^2\begin{bmatrix}+\left(B_{11}+B_{12}\right)U_{0b}\alpha^6+B_{11}U_{0b}\beta^6+\left(B_{11}+2B_{12}+4B_{33}\right)U_{0b}\alpha^4\beta^2\\+\left(B_{11}+B_{12}+4B_{33}\right)U_{0b}\alpha^2\beta^4\\+\left(D_{11}+D_{12}\right)U_{0s}\alpha^6+D_{11}U_{0s}\beta^6+\left(D_{11}+D_{12}+4D_{33}\right)U_{0s}\alpha^2\beta^4\\+\left(D_{11}+2D_{12}+4D_{33}\right)U_{0s}\alpha^4\beta^2\end{bmatrix}\\
&-H_{33}U_{0s}\left(\alpha^2+\beta^2\right)+\frac{16Q_0}{\pi^2rg}+N_0\left(U_{0b}+U_{0s}\right)\left(\alpha^2+\beta^2\right)=0
\end{aligned}
\tag{17b}
$$

where $\alpha=r\pi/a,\beta=g\pi/b$. Alternatively, express in a more concise manner:

$$
\begin{bmatrix}C_{11}&C_{12}\\C_{21}&C_{22}\end{bmatrix}\begin{Bmatrix}U_{0b}\\U_{0s}\end{Bmatrix}=\frac{16Q_0}{\pi^2rg}\begin{Bmatrix}1\\1\end{Bmatrix}
\tag{18}
$$

where

$$
\begin{aligned}
C_{11}&=2\left(2A_{33}+A_{12}\right)\alpha^2\beta^2\\
&\quad+A_{11}\left(\beta^4+\alpha^4\right)\\
&\quad+l^2\begin{bmatrix}\left(A_{11}+A_{12}\right)\alpha^6+A_{11}\beta^6+\left(A_{11}+2A_{12}+4A_{33}\right)\alpha^4\beta^2\\+\left(A_{11}+A_{12}+4A_{33}\right)\alpha^2\beta^4\end{bmatrix}\\
C_{12}&=2\left(2B_{33}+B_{12}\right)\alpha^2\beta^2\\
&\quad+B_{11}\left(\beta^4+\alpha^4\right)\\
&\quad+l^2\begin{bmatrix}\left(2B_{12}+B_{11}+4l^2B_{33}\right)\alpha^4\beta^2+\left(B_{12}+B_{11}+4l^2B_{33}\right)\alpha^2\beta^4\\+\left(B_{12}+B_{11}\right)\alpha^6+B_{11}\beta^6\end{bmatrix}
\end{aligned}
\tag{19a}
$$

$$
\begin{aligned}
C_{21}&=2\left(B_{12}+2B_{33}\right)\alpha^2\beta^2\\
&\quad+B_{11}\left(\alpha^4+\beta^4\right)\\
&\quad+l^2\begin{bmatrix}\left(B_{11}+B_{12}+4B_{33}\right)\alpha^2\beta^4+\left(B_{11}+2B_{12}+4B_{33}\right)\alpha^4\beta^2\\+\left(B_{11}+B_{12}\right)\alpha^6+B_{11}\beta^6\end{bmatrix}\\
C_{22}&=\left(D_{11}+H_{33}l^2\right)\left(\alpha^4+\beta^4\right)+2\left(D_{12}+2D_{33}+H_{33}l^2\right)\alpha^2\beta^2\\
&\quad+H_{33}U_{0s}\left(\alpha^2+\beta^2\right)\text{-}N_0\left(\alpha^2+\beta^2\right)\\
&\quad+l^2\begin{bmatrix}+\left(D_{11}+D_{12}+4D_{33}\right)\alpha^2\beta^4+\left(D_{11}+2D_{12}+4D_{33}\right)\alpha^4\beta^2\\+\left(D_{11}+D_{12}\right)\alpha^6+D_{11}\beta^6\end{bmatrix}
\end{aligned}
\tag{19b}
$$

$$\alpha=r\pi/a,\beta=g\pi/b$$

By solving the above system of equations, one may get the values of U_{0b} and U_{0s}, which will then be used to calculate the displacement w_z of the plate.

The equilibrium equation of the plate for the static buckling issue, without considering the effect of external force q, may be expressed as:

$$\begin{bmatrix} C_{11} & C_{12} \\ C_{21} & C_{22} \end{bmatrix} \begin{Bmatrix} U_{0b} \\ U_{0s} \end{Bmatrix} = \begin{Bmatrix} 0 \\ 0 \end{Bmatrix} \tag{20}$$

where

$$\begin{aligned} C_{11} &= -N_0\left(\alpha^2+\beta^2\right)+2\left(2A_{33}+A_{12}\right)\alpha^2\beta^2 \\ &\quad +A_{11}\left(\beta^4+\alpha^4\right) \\ &\quad +l^2\begin{bmatrix}\left(A_{11}+A_{12}\right)\alpha^6+A_{11}\beta^6+\left(A_{11}+2A_{12}+4A_{33}\right)\alpha^4\beta^2 \\ +\left(A_{11}+A_{12}+4A_{33}\right)\alpha^2\beta^4\end{bmatrix} \\ C_{12} &= -N_0\left(\alpha^2+\beta^2\right)+2\left(2B_{33}+B_{12}\right)\alpha^2\beta^2 \\ &\quad +B_{11}\left(\beta^4+\alpha^4\right) \\ &\quad +l^2\begin{bmatrix}\left(2B_{12}+B_{11}+4l^2B_{33}\right)\alpha^4\beta^2+\left(B_{12}+B_{11}+4l^2B_{33}\right)\alpha^2\beta^4 \\ +\left(B_{12}+B_{11}\right)\alpha^6+B_{11}\beta^6\end{bmatrix} \end{aligned} \tag{21a}$$

$$\begin{aligned} C_{21} &= -N_0\left(\alpha^2+\beta^2\right)+2\left(B_{12}+2B_{33}\right)\alpha^2\beta^2 \\ &\quad +B_{11}\left(\alpha^4+\beta^4\right) \\ &\quad +l^2\begin{bmatrix}\left(B_{11}+B_{12}+4B_{33}\right)\alpha^2\beta^4+\left(B_{11}+2B_{12}+4B_{33}\right)\alpha^4\beta^2 \\ +\left(B_{11}+B_{12}\right)\alpha^6+B_{11}\beta^6\end{bmatrix} \\ C_{22} &= \left(D_{11}+H_{33}l^2\right)\left(\alpha^4+\beta^4\right)+2\left(D_{12}+2D_{33}+H_{33}l^2\right)\alpha^2\beta^2 \\ &\quad +H_{33}U_{0s}\left(\alpha^2+\beta^2\right)-N_0\left(\alpha^2+\beta^2\right) \\ &\quad +l^2\begin{bmatrix}+\left(D_{11}+D_{12}+4D_{33}\right)\alpha^2\beta^4+\left(D_{11}+2D_{12}+4D_{33}\right)\alpha^4\beta^2 \\ +\left(D_{11}+D_{12}\right)\alpha^6+D_{11}\beta^6\end{bmatrix} \end{aligned} \tag{21b}$$

$$\alpha = r\pi/a, \beta = g\pi/b$$

By solving the system of equations (20), we can get the value of N_0, which is contingent upon the values of two parameters, r and g. The minimum value of N_0 represents the critical buckling load of the nanoplate.

3. VERIFICATION

Verification example 1: The nanoplate has equal sides of 10nm each, a thickness of 0.34 nm, a Poisson's ratio of 0.3, a Young's modulus of 1100 GPa. The plate is supported by a load that is evenly distributed with an intensity of q_0. The parameter used for computation and

comparison is the displacement at the center of the plate, which is standardized using the following formula

$$w_{max} = \frac{1000D}{a^4 q_0} w_z\left(\frac{a}{2}, \frac{b}{2}\right) \tag{22}$$

where $D = \frac{Eh^3}{12\left(1-\nu^2\right)}$. The computation and juxtaposition outcomes are shown in Table 1. The findings of this study demonstrate a high degree of correlation between the calculated results obtained in this work and those obtained using the finite element approach [30] and the solution method [31]. This demonstrates the dependability of the computational theory.

Table 1. Comparison of the deflection w_{max} of the nanoplate.

Nonlocal Term	**Method**	***l* (nm)**			
		0	0.2	0.5	1
Positive	FEM [30]	4.062	4.092	4.252	-
	Exact [31]	4.062	4.091	4.260	-
	This work	4.079	4.107	4.258	-
Negative	FEM [30]	4.062	4.033	3.885	3.427
	Exact [31]	4.062	4.033	3.884	3.423
	This work	4.079	4.050	3.904	3.444

Verification example 2: The square plate has a side length of *a*, a thickness of *h* = 0.34 nm, a Young's modulus of 30 MPa, and a Poisson's ratio of 0.3. The critical buckling load parameter is normalized as follows:

$$T_{bl} = N_0 \frac{a^2}{\pi^2 D_{buck}},\ D_{buck} = \frac{Eh^3}{12\left(1-\nu^2\right)} \tag{23}$$

Table 2 displays the findings of analyzing the critical buckling load of the compressed plate on all four sides. The calculations for documents [28], [32–33] were done using analytical techniques. Based on the comparing data, it can be inferred that the computation approach used in this study guarantees dependability.

Table 2. Examine the buckling load of the plate when subjected to compression from all four sides.

Method	***a*/*h*=10**	***a*/*h*=20**	***a*/*h*=30**
Exact [28]	1.893	1.972	1.987
Exact [32]	1.893	1.972	1.987
Exact [33]	1.893	1.972	1.987
This work	1.893	1.972	1.987

4. NUMERICAL RESULTS

This part presents the findings of calculations for the static bending and buckling issue of organic nanoplates, in addition to the previously discussed theory. The ratio *b*/*a* takes on the values 0.5-3, The thickness is *h*, and the values of the *a*/*h* are from 10 to 50. This plate has five layers. The ratio of the thicknesses of the layers is 550/0.120/0.050/0.170/0.100. Table 3 provides a comprehensive overview of the mechanical properties associated with each

individual material layer. The total thickness, denoted as *h*, remains constant at a value of 0.55044 nm for all computational instances.

Table 3. Properties of specific layers in organic nanoplates [11].

Order of layer	Layer name	Modulus of Young	Mass density	Ratio of Poisson
First layer	Glass	69	2400	0.23
Second layer	ITO	116	7120	0.35
Third layer	PEDOT: PSS	2.3	1000	0.4
Fourth layer	P3HT: PCBM	6	1200	0.23
Fifth layer	Aluminum	70	2601	0.35

The plate is supported by a load that is evenly distributed with an intensity of q_0. The parameter used for computation is the greatest deflection in the center of the plate, determined using a dimensionless formula as follows:

$$w_{max} = 10^3 \frac{D_{ogarnic}}{a_0^4 q_0} w_z \left(\frac{a}{2}, \frac{b}{2} \right) \tag{24}$$

in which $D_{ogarnic} = \frac{E_{Al} h^3}{12\left(1-\nu^2\right)}$ and $a_0 = 10h$.

To address the issue of plate buckling, the critical buckling load of the plate is determined using a dimensionless formula, as shown below:

$$T_{bl} = N_0 \frac{a^2}{\pi^2 D_{ogarnic}} \tag{25}$$

Table 4. The maximum deflection of the plate depends on the plate thickness, *b*/*a*=1.

Nonlocal Term	*a*/*h*	*l*/*h*				
		0	0.2	0.5	0.6	0.7
Positive	10	4.648	4.680	4.849	4.938	5.059
	20	71.906	72.032	72.696	73.046	73.460
	30	361.716	361.999	363.485	364.265	365.188
	50	2781.898	2782.681	2786.795	2788.951	2791.502
Negative	10	4.648	4.616	4.451	4.368	4.272
	20	71.906	71.780	71.123	70.781	70.379
	30	361.716	361.434	359.955	359.183	358.272
	50	2781.898	2781.115	2777.009	2774.86	2772.323

The maximum bending deflection of the organic plate is determined by the plate thickness and the ratio of the lengths of its two sides, as shown in Tables 4–5. Observations indicate that:

+ As the plate becomes thinner and the ratio of its edge lengths grows, the plate's stiffness reduces and the maximum displacement of the plate increases.

+ When the positive nonlocal coefficient is present, increasing the parameter *l* results in an increase in the maximum displacement of the plate. This demonstrates that the parameter *l* decreases the stiffness of the structure.

+ When the parameter *l* grows in the case of the negative nonlocal coefficient, the maximum displacement of the plate decreases. This demonstrates that the parameter *l* enhances the stiffness of the structure.

Table 5. The maximum deflection of the plate depends on the ratio of the lengths of the two sides of the plate, *a*/*h*=10.

Nonlocal Term	***b*/*a***	***l*/*h***				
		0	0.2	0.5	0.6	0.7
Positive	0.5	0.768	0.780	0.744	0.926	0.945
	1	4.648	4.680	4.849	4.938	5.059
	2	11.351	11.407	11.701	11.856	12.035
	3	13.526	13.588	13.920	14.095	14.298
Negative	0.5	0.768	0.755	0.694	0.665	0.634
	1	4.648	4.616	4.451	4.368	4.272
	2	11.351	11.296	11.013	10.868	10.701
	3	13.526	13.464	13.146	12.984	12.797

The critical buckling load of organic plates was calculated for several scenarios. Tables 6–7 show the findings for the situation where the *a*/*h* ratio ranges from 10 to 50, and the *b*/*a* ratio ranges from 0.5 to 3. The outcome indicates that:

+ By increasing the ratios of *a*/*h* and *b*/*a*, the stiffness of the plate lowers, resulting in a drop in the critical buckling load of the organic plate. Consequently, the working performance of the plate reduces.

+ When the nonlocal coefficient is positive, raising the parameter *l* leads to a drop in the critical buckling load of the plate. Consequently, the compressive capacity of the plate also decreases. However, when the nonlocal coefficient is negative, increasing the parameter *l* leads to an increase in the critical buckling load of the plate. This indicates an increase in the working performance of the organic plate.

Table 6. The critical buckling load of the plate depends on the plate thickness, *b*/*a*=1.

Nonlocal Term	***a*/*h***	***l*/*h***				
		0	0.2	0.5	0.6	0.7
Positive	10	1.736	1.722	1.650	1.613	1.568
	20	0.450	0.449	0.445	0.442	0.439
	30	0.2016	0.2015	0.2005	0.2001	0.1995
	50	0.07287	0.07285	0.07273	0.07266	0.07259
Negative	10	1.736	1.750	1.822	1.860	1.904
	20	0.450	0.451	0.456	0.458	0.461
	30	0.2016	0.2018	0.2028	0.2032	0.2038
	50	0.07287	0.07289	0.07301	0.07308	0.07315

Table 7. The critical buckling load of the plate depends on the ratio of the lengths of the two sides of the plate, a/h=10.

Nonlocal Term	***b/a***	***l/h***				
		0	0.2	0.5	0.6	0.7
Positive	0.5	4.046	3.968	3.559	3.345	3.091
	1	1.736	1.722	1.650	1.613	1.568
	2	1.105	1.099	1.067	1.051	1.031
	3	0.9861	0.9811	0.9547	0.9409	0.9246
Negative	0.5	4.046	4.124	4.533	4.747	5.000
	1	1.736	1.750	1.822	1.860	1.904
	2	1.105	1.111	1.143	1.159	1.179
	3	0.9861	0.991	1.017	1.031	1.047

5. CONCLUSIONS

This work has provided a precise solution to the issue of static bending and static buckling of organic nanoplates. The plate's balancing equation is formulated based on the novel third-order shear deformation theory. Based on the computation findings, this study has drawn some key conclusions: As the plate becomes thinner and the thickness ratio between the two sides of the plate grows, the plate's stiffness reduces, the maximum deflection of the plate increases, and the critical buckling load of the plate lowers. If the coefficient is positive and nonlocal, increasing the parameter l results in a higher maximum deflection of the plate and a fall in the critical buckling load. This indicates a loss in the working performance of the plate. However, when the nonlocal coefficient is negative, the plate's working performance is enhanced as the parameter l grows. However, in order to validate the computed model against the real model, it is necessary to conduct experiments for testing, hence establishing a foundation for practical design of organic plates.

REFERENCES

[1]. H. Hoppe, N. S. Sariciftci, Organic solar cells: An overview, J. Mater. Res., 19 (2004) 1924–1945. https://doi.org/10.1557/JMR.2004.0252.

[2]. I. Cardinaletti, T. Vangerven, S. Nagels, R. Cornelissen, D. Schreurs, J. Hruby, J. Vodnik, D. Devisscher, J. Kesters, J. D.Haen, A. Franquet, V. Spampinato, T. Conard, W.Maes, W. Deferme, J V. Manca, Organic and perovskite solar cells for space applications, Sol. Energy Mater. Sol. Cells, 182 (2018) 121–127. https://doi.org/10.1016/j.solmat.2018.03.024.

[3]. Z. Wu, Y. Zhang, Z. Huan, Solving Post-Buckling Characteristic of Thermal-Resistance Films Attached to Glass Façade via an Optimization Method, Int. J. Struct. Stab. Dyn, 19 (2019). https://doi.org/10.1142/S0219455419500688.

[4]. F. Nehm, T. Pfeiffelmann, F. Dollinger, L. Müller-Meskamp, K. Leo, Influence of aging climate and cathode adhesion on organic solar cell stability, Sol. Energy Mater. Sol. Cells, 168, (2017) 1–7. https://doi.org/10.1016/j.solmat.2017.03.037.

[5]. M. Tavakkoli, R. Ajeian, M. Nakhaee Badrabadi, S. Saleh Ardestani, S. M. H. Feiz, K. Elahi Nasab, Progress in stability of organic solar cells exposed to air, Sol. Energy Mater. Sol. Cells, 95 (2011) 1964–1969. https://doi.org/10.1016/j.solmat.2011.01.029.

[6]. T. F. O'Connor, A.V. Zaretski, S. Savagatrup, A.D. Printz, C.D. Wilkes, M.I. Diaz, E.J. Sawyer, D. J. Lipomi, Wearable organic solar cells with high cyclic bending stability: Materials selection criteria, Sol. Energy Mater. Sol. Cells, 144 (2016) 438–444. https://doi.org/10.1016/j.solmat.2015.09.049.

[7]. Y. L. Pei, P. S. Geng, L. X. Li, A modified higher-order theory for FG beams, Eur. J. Mech.

A/Solids, 72 (2018) 186–197. https://doi.org/10.1016/j.euromechsol.2018.05.008.
[8]. A. Cemal Eringen, Nonlocal polar elastic continua, Int. J. Eng. Sci., pp. 1–16, 1972.
[9]. F. Yang, A. C. M. Chong, D. C. C. Lam, P. Tong, Couple stress based strain gradient theory for elasticity, Int. J. Solids Struct., 39 (2002) 2731–2743. https://doi.org/10.1016/S0020-7683(02)00152-X.
[10].D. C. C. Lam, F. Yang, A. C. M. Chong, J. Wang, P. Tong, Experiments and theory in strain gradient elasticity, J. Mech. Phys. Solids, 51 (2003) 1477–1508. https://doi.org/10.1016/S0022-5096(03)00053-X.
[11].Q. Li, D. Wu, W. Gao, F. Tin-Loi, Z. Liu, J. Cheng, Static bending and free vibration of organic solar cell resting on Winkler-Pasternak elastic foundation through the modified strain gradient theory, Eur. J. Mech. A/Solids, 78 (2019) 103852. https://doi.org/10.1016/j.euromechsol.2019.103852.
[12].Q. Li, D. Wu, W. Gao, F. Tin-Loi, Size-dependent instability of organic solar cell resting on Winkler–Pasternak elastic foundation based on the modified strain gradient theory, Int. J. Mech. Sci., 177 (2020). https://doi.org/10.1016/j.ijmecsci.2019.105306.
[13].N. D. Duc, K. Seung-Eock, T. Q. Quan, D. D. Long, V. M. Anh, Nonlinear dynamic response and vibration of nanocomposite multilayer organic solar cell, Compos. Struct., 184 (2018) 1137–1144. https://doi.org/10.1016/j.compstruct.2017.10.064.
[14].S. Liu, K. Wang, B. Wang, J. Li, C. Zhang, Size effect on thermo-mechanical instability of micro/nano scale organic solar cells, Meccanica, 57 (2022) 87–107. https://doi.org/10.1007/s11012-021-01411-6.
[15].M. K. Hamed, T. Masoud, A size-dependent study on buckling and post-buckling behavior of imperfect piezo-flexomagnetic nano-plate strips, Adv. in nano research, 12 (2022) 427-440. https://doi.org/10.12989/anr.2022.12.4.427.
[16].A. Naderi, The nonlocal parameter for three-dimensional nonlocal elasticity analyses of square graphene sheets: An exact buckling analysis, Proc. Inst. Mech. Eng Part N, 236 (2022) 41-48. https://doi.org/10.1177/2397791421102982
[17].I. Esen, R. Özmen, Thermal vibration and buckling of magneto-electro-elastic functionally graded porous nanoplates using nonlocal strain gradient elasticity, Comp. Struct, 296 (2022) 115878. https://doi.org/10.1016/j.compstruct.2022.115878
[18].Q. Jin, Y. Ren, Nonlinear size-dependent bending and forced vibration of internal flow-inducing pre- and post-buckled FG nanotubes, Comm. Nonl. Science Num. Sim, 104 (2022) 106044. https://doi.org/10.1016/j.cnsns.2021.106044
[19].T. Hai, M. M. Al-Masoudy, S. Alsulamy, M. H. E. Ouni, A. Ayvazyan, A. Kumar, Moving load analysis on cross/angle-ply laminated composite nanoplates resting on viscoelastic foundation, Comp. Struct, 305 (2023) 116540. https://doi.org/10.1016/j.compstruct.2022.116540
[20].B. V. Tuyen. Free Vibration Behaviors of Nanoplates Resting on Viscoelastic Medium. Arabian J. Science Eng, 48 (2023) 11511–11524. https://doi.org/10.1007/s13369-022-07500-2
[21].P.H. Wan, M.S.H. Al-Furjan, R. Kolahchi, L. Shan, Application of DQHFEM for free and forced vibration, energy absorption, and post-buckling analysis of a hybrid nanocomposite viscoelastic rhombic plate assuming CNTs' waviness and agglomeration, Mech. Syst. Sign. Proc, 189 (2023) 110064. https://doi.org/10.1016/j.ymssp.2022.110064
[22].D. T. Luat, D. Van Thom, T. T. Thanh, P. Van Minh, T. Van Ke, P. V. Vinh, Mechanical analysis of bi-functionally graded sandwich nanobeams, Adv. Nano Res., 11 (2021) 55–71. https://doi.org/10.12989/anr.2021.11.1.055.
[23].D. H. Duc, D. Van Thom, P. H. Cong, P. Van Minh, N. X. Nguyen, Vibration and static buckling behavior of variable thickness flexoelectric nanoplates, Mech. Based Des. Struct. Mach, 51 (2022) 7102-7130. https://doi.org/10.1080/15397734.2022.2088558
[24].D. H. Doan, A. M. Zenkour, D. Van Thom, Finite element modeling of free vibration of cracked nanoplates with flexoelectric effects, Eur. Phys. J. Plus, 137 (2022). https://doi.org/10.1140/epjp/s13360-022-02631-9.
[25].D. N. Thai, P. Van Minh, C. Phan Hoang, T. Ta Duc, N. Nguyen Thi Cam, D. Nguyen Thi, Bending of Symmetric Sandwich FGM Beams with Shear Connectors, Math. Probl. Eng, 2021 (2021).

https://doi.org/10.1155/2021/7596300.
[26].D. V. Thom, D. H. Duc, P. V. Minh, N. S. Tung, Finite Element Modelling for Free Vibration Response of Cracked Stiffened Fgm Plates," Vietnam J. Sci. Technol., 58 (2020) 119. https://doi.org/10.15625/2525-2518/58/1/14278.
[27].P. V. Vinh, N. T. Dung, N. C. Tho, D. V. Thom, L. K. Hoa, Modified single variable shear deformation plate theory for free vibration analysis of rectangular FGM plates, Struct., 29 (2021) 1435-1444. https://doi.org/10.1016/j.istruc.2020.12.027.
[28].D. M. Tien, D. V. Thom, N. T. H. Van, A. Tounsi, P. V. Minh, D. N. Mai, Buckling and forced oscillation of organic nanoplates taking the structural drag coefficient into account, Comp. Concr, 32 (2023) 553-565. https://doi.org/10.12989/cac.2023.32.6.553
[29].R. P. Shimpi, Refined plate theory and its variants, AIAA J, 40 (2002) 137–146. https://doi.org/10.2514/3.15006.
[30].B. Babu, B.P. Patel, A new computationally efficient finite element formulation for nanoplates using secondorder strain gradient Kirchhoff's plate theory, Comp. Part B: Engineering, 168 (2019) 302-311. https://doi.org/10.1016/j.compositesb.2018.12.066
[31]. R. Ansari, R. Gholami, H. Rouhi, Vibration analysis of single-walled carbon nanotubes using different gradient elasticity theories, Comp. Part B: Engineering, 43 (2012) 2985-2989. https://doi.org/10.1016/j.compositesb.2012.05.049.
[32].M. Sobhy, Natural frequency and buckling of orthotropic nanoplates resting on two-parameter elastic foundations with various boundary conditions, J. Mechanics 30 (2014) 443–453. https://doi.org/10.1017/jmech.2014.46
[33].M. Sobhy, A. F. Radwan, A New Quasi 3D Nonlocal Plate Theory for Vibration and Buckling of FGM Nanoplates. International Journal of Applied Mechanics, 9 (2017) 1750008. https://doi.org/10.1142/S1758825117500089